Journal of Alloys and Compounds 591 (2014) 268–274

Contents lists available at ScienceDirect

Journal of Alloys and Compounds

journal homepage: www.elsevier.com/locate/jalcom

Crystallization kinetics of a barium–zinc borosilicate glass by a non-isothermal method

A.A.S. Lopes [a], R.C.C. Monteiro [a,*], R.S. Soares [a], M.M.R.A. Lima [a], M.H.V. Fernandes [b]

[a] *CENIMAT/I3N, Department of Materials Science, Faculty of Sciences and Technology, Universidade Nova de Lisboa, 2829-516 Caparica, Portugal*
[b] *CICECO and Department of Ceramics and Glass Engineering, University of Aveiro, Campus Universitário de Santiago, 3810-193 Aveiro, Portugal*

ARTICLE INFO

Article history:
Received 24 July 2013
Received in revised form 15 November 2013
Accepted 10 December 2013
Available online 16 December 2013

Keywords:
Differential thermal analysis
Borosilicate glasses
Non-isothermal process
Crystallization kinetics

ABSTRACT

The crystallization kinetics of a glass with a molar composition $40BaO–20ZnO–30B_2O_3–10SiO_2$ was investigated. The kinetic parameters, activation energy for crystallization (E_c) and Avrami exponent (n), were evaluated under non-isothermal conditions using the results obtained by differential thermal analysis (DTA) performed at different heating rates. DTA curves exhibited two overlapping exothermic peaks associated with the crystallization of the glass. Barium borate (BaB_4O_7) was the first crystalline phase to be formed and it was followed by the formation of barium zinc silicate ($BaZnSiO_4$), as identified by XRD. For the first exothermic peak, when the fraction of crystallization (χ) increased from 0.1 to 0.9, the local activation energy ($E_c(\chi)$) decreased from 700 to 500 kJ/mol, while for the second exothermic peak, $E_c(\chi)$ slightly increased from 490 to 570 kJ/mol. For the range of $0.1 < \chi < 0.9$, the local Avrami exponent ($n(\chi)$) increased from ~1 to 1.4 for the first exothermic peak and it decreased from ~1.7 to 1.4 for the second exothermic peak. Observation by SEM of the microstructure of sintered glass samples revealed that crystallization started at the surface of glass particles, with growth of lamellar crystallites, that together with some quasi-spherical nano-sized crystallites progressed towards the inside of the glass at the highest sintering temperatures. The change of the local activation energy with the fraction of crystallization suggested that a multi-step kinetic reaction took place during sintering and crystallization of the glass.

1. Introduction

Borosilicate glasses are considered promising candidates for different applications in electronic industries, such as display panels, low-temperature co-fired ceramics and packaging, due to their low softening temperature, low dielectric constant, and high electrical resistance [1–4]. In order to decrease the sintering temperature of these glasses, some alkali or bivalent metal oxides must be added, often at the expense of dielectric properties as well as crystallization behavior [5,6].

Lead borosilicate glasses became popular as commercial low-temperature sinterable glasses due to their low glass transition temperature (T_g), high structural stability, and good electrical and thermal characteristics [7]. As lead is a component with deleterious health and environmental effects during processing, environmental-friendly lead-free borosilicate glasses have been developed, with barium and zinc substitution for lead. However, in this case, to obtain glasses with low T_g, significant amount of a glass network modifier is necessary, which almost inevitably results in the crystallization of the glass [1–6,8]. The final properties of the sintered glass will be controlled by the degree of crystallization that occurs during firing [6]. Therefore, a thorough understanding of the crystallization kinetics and mechanisms of nucleation and growth is needed in order to optimize the processing parameters.

Different methods have been proposed to study the crystallization kinetics of glasses. Thermoanalytical techniques such as differential thermal analysis (DTA) and differential scanning calorimetry (DSC) have been frequently used for such studies, allowing the possibility of obtaining useful data with isothermal and non-isothermal methods [9–14]. Johnson–Mehl–Avrami (JMA) model, that defines an effective crystallization rate constant having an Arrhenius temperature dependence, is generally used for the kinetic analyses of isothermal thermoanalytical data [12,15]. In this method, glass samples are quickly heated and soaked at a temperature above T_g, and hence crystallization occurs at a fixed temperature. In non-isothermal method, glass samples are heated at a certain heating rate and crystallized during the thermal analysis scan. The non-isothermal method is more simple and faster than the isothermal method [12,13].

The most important kinetic parameters for the crystallization of glasses are the activation energy and the Avrami exponent that depends on the mechanism and dimensionality of the crystal growth. These parameters can be determined from experimental results obtained from non-isothermal thermoanalytical studies

---

[*] Corresponding author. Tel.: +351 212948564; fax: +351 212957810.
E-mail address: rcm@fct.unl.pt (R.C.C. Monteiro).

0925-8388/$ - see front matter © 2013 Elsevier B.V. All rights reserved.
http://dx.doi.org/10.1016/j.jallcom.2013.12.086

using different methods, such as those proposed by Kissinger [15], Ozawa [16] and Augis and Bennett [17]. Most of the different equations that have been proposed to interpret non-isothermal data assume that the variation of the peak crystallization temperature is directly related to the heating rate employed in the experiment [15–19].

Few investigations have been performed on the crystallization kinetics of glasses based on the quaternary system BaO–ZnO–B_2O_3–SiO_2. Recently, studies on the crystallization kinetics of glasses based on the molar composition 30BaO–20ZnO–$x$$M_2O_3$–(10−$x$)$B_2O_3$–40$SiO_2$, where M = Al, Mn, and developed to be used as glass sealants for solid oxide fuel cells, have been reported [10,20–22]. In the present work, the crystallization kinetics of a glass with a different composition, 40BaO–20ZnO–30B_2O_3–10SiO_2 (mol%), has been investigated under non-isothermal conditions by DTA. The aim of this study was to determine the temperature of maximum crystallization rate and the kinetic parameters, and to identify the crystallization sequences of the glass. The development of the crystalline phases after heat treatment of the glass at different temperatures was investigated by XRD and the microstructure of the crystalline phases was observed by SEM. The nucleation and growth of crystalline phases in glass matrix is described and analysed.

2. Experimental procedure

The glass was prepared from $BaCO_3$ (BDH), ZnO (Merck), H_3BO_3 (Merck) and SiO_2 (BDH) powders, all of them with a purity higher than 99%. An homogeneous mixture of a 20 g batch was prepared by weighing the right amounts of the starting materials, mixing for 30 min in a Teflon jar, using a laboratory powder mixer (turbula WAB, T2F), and then melting in platinum crucible in an electric furnace at 1723 K for 2 h in air. The molten glass was quenched into cold distilled water to form a glass frit. The glass frit (approximately 20 g) was dried and milled with absolute ethanol for 2 h using an agate ball mill (Fritsch, Pulverizette), with a 80 ml capacity container and agate balls (3 balls of ∅ 20 mm and 5 balls of ∅ 10 mm, weight ratio of sample/balls = 0.5) rotating at constant speed of 600 rpm. Then, the milled glass was dried again and sieved to obtain a glass powder with a particle size smaller than 65 μm. After sieving, the particle size distribution of the powder was evaluated using a laser diffraction particle size analyzer (Coulter LS 230). The as-prepared glass powder had a mean particle of 14.5 μm and a particle size distribution as presented in Fig. 1.

Differential thermal analysis (DTA) of the glass powder was performed using a Linseis STA PT1600 equipment. DTA runs were performed using 50 mg glass powder samples heated in alumina crucible from room temperature to 973 K, in static air, at various heating rates (5, 10, 15 and 20 K/min). Measured DTA data were corrected by subtracting a blank measurement made without sample under the same conditions, and automatic baseline correction was performed with the software package delivered with the thermal analysis equipment. The glass transition temperature (T_g), the onset crystallization temperature (T_c) and the peak crystallization temperature (T_p) were determined using the software associated to the equipment, and the measurement error is assumed as 1%.

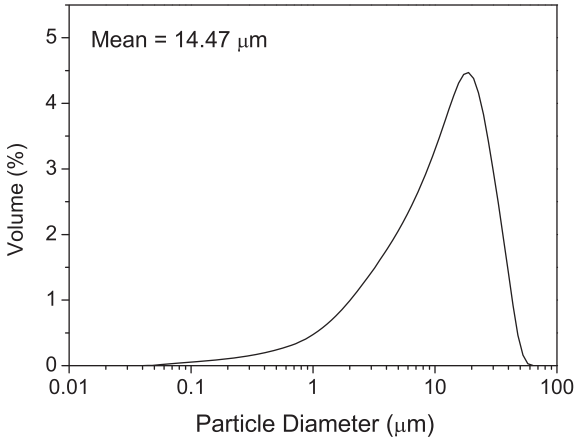

Fig. 1. Particle size distribution of glass powder used for differential thermal analysis and to prepare the glass-powder compacts.

The amorphous nature of the as-prepared glass powder and the crystalline phases formed in heat-treated glass samples were identified by X-ray diffraction analysis (XRD), using a DMAX-IIIC diffractometer-Rigaku Industrial Corporation, with Cu Kα radiation (40 kV, 30 mA), 2θ angle range 10–60°, a scanning rate of 2° min^{-1} and a sampling interval of 0.01° (2θ). The phases were identified by comparing the experimental X-ray patterns to standards complied by the International Centre for Diffraction Data (ICDD). No crystallinity was detected by XRD in the as-prepared glass powder.

The heat-treated samples used in this study were prepared by uniaxial pressing the glass powder under a compressive stress of ~75 MPa and firing the resulting compacts (≈3 mm height, 13 mm diameter) in an electric tubular furnace from room temperature up to a selected temperature suggested by the DTA results. The samples were held during 1 h at that temperature and then were left to cool inside the furnace. The microstructure of sintered glass samples was observed using a scanning electron microscope, SEM (ZEISS, DSM 960). SEM observations were carried out in polished surfaces (mirror finishing) that were etched by immersion in 2 vol.% HF solution for 2 s.

3. Results and discussion

3.1. Thermal and structural characterization

The DTA curves for the glass powder obtained at different heating rates are presented in Fig. 2. The DTA curves show a first exothermic effect followed by a strong exothermic peak, which are partially overlapped. Fig. 3 shows the crystallization exotherms for the DTA curve obtained at a heating rate (β) of 10 K/min together with an inset where the separation of the two overlapping crystallization peaks is illustrated. The software used for exotherm peak fitting was OriginPro 8. Modeling of the experimental DTA curve was carried out using two partially overlapping Gaussian curves. The characteristic temperatures of the glass (T_g, T_c and T_p) increased with the increase in heating rate, as shown in Table 1. It is observed that the temperature gap (T_c–T_g), which corresponds to the interval in which structural rearrangements are allowed without the occurrence of crystallization, is smaller than 100 K. This is in agreement with the results obtained in a previous work by some of the authors [6], where the crystallization and densification behavior of different borosilicate glasses with high BaO and ZnO content were characterized.

Fig. 4 presents the XRD patterns for the glass samples heated at 10 K/min from room temperature to the indicated temperature and held at each temperature for 1 h. These results show that no crystallization is observed for samples heated at $T = 793$ K ($T_g < T < T_c$, for all β), while a crystalline phase, barium borate, BaB_4O_7 (JCPDS card No. 15-860), is identified after heating at $T = 833$ K ($T_c < T < T_{p1}$, for all β), and the presence of an extra crystalline phase, barium zinc silicate, $BaZnSiO_4$ (JCPDS card No. 42-337), is identified in samples heated at 843 K. From this figure, it appears that

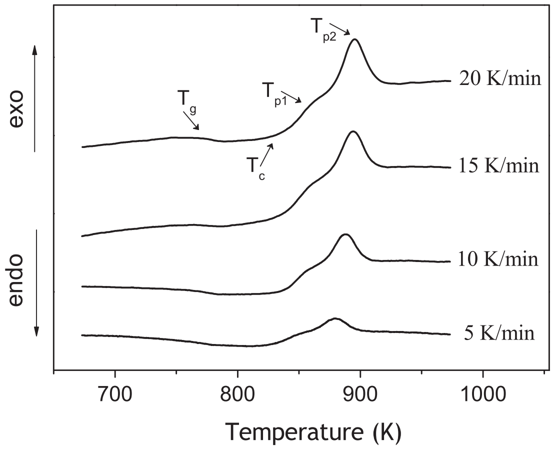

Fig. 2. DTA curves for the glass powder obtained at different heating rates.

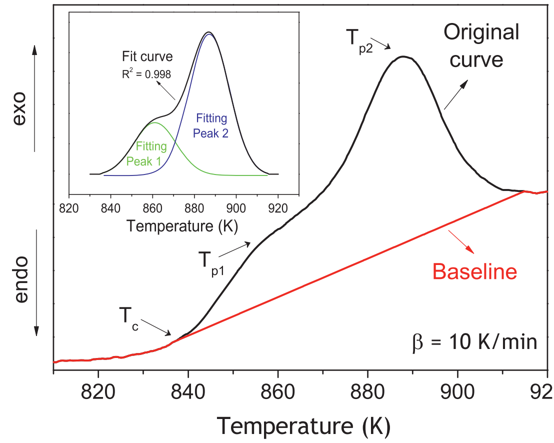

Fig. 3. DTA curve obtained at $\beta = 10$ K/min. The inset depicts the separation of the overlapped crystallization peaks in the crystallization exotherm.

Table 1
Glass transition temperature (T_g), onset crystallization temperatures (T_{c1} and T_{c2}) and maximum crystallization temperatures (T_{p1} and T_{p2}) determined from DTA data obtained at different heating rates.

Heating rate, β (K/min)	T_g (K)	Peak 1		Peak 2	
		T_{c1} (K)	T_{p1} (K)	T_{c2} (K)	T_{p2} (K)
5	720	819	852	837	879
10	751	837	861	847	887
15	764	838	865	851	893
20	769	840	866	854	895

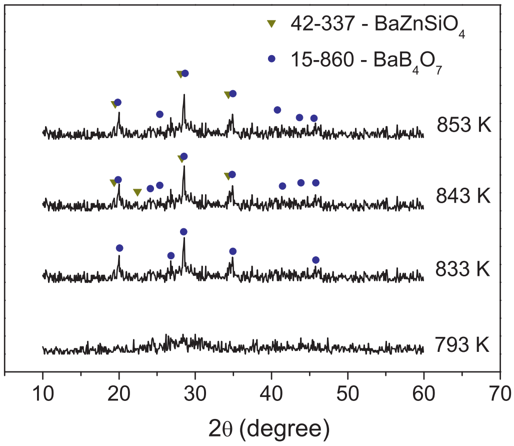

Fig. 4. XRD patterns of the glass samples heat-treated at various temperatures.

increasing the treatment temperature from 843 K to 853 K, the relative intensity of the main diffraction peaks of each crystalline phase is not affected. The above results indicate that the formation of the two crystalline phases can be ascribed to the two overlapping crystallization peaks in the DTA curves: the first exothermic peak is attributed to the crystallization of BaB_4O_7 and the second to the formation of $BaZnSiO_4$.

In a recent paper [6], some of us reported the formation of another barium borate phase, β-BaB_2O_4 (JCPDS card No. 80-1489), in glass compositions based on the same system but having a higher BaO content (50 and 60 mol%) than the present studied glass (40 mol%). The precipitation of the two barium borate phases, BaB_4O_7 and β-BaB_2O_4, in heat-treated powdered glass samples based on the system BaO–B_2O_3–TiO_2 has been described by some authors [23]. In such a system, an extra phase, $BaTi(BO_3)_2$ was also identified and the dependence of phase formation on the composition of the crystallized samples been emphasized [23].

3.2. Crystallization kinetics

The kinetic parameters of the glass crystallization, activation energy (E_c) and Avrami exponent (n), were determined using different methods. The activation energy for crystallization (E_c) was determined according to the Kissinger method, considering the heating rate dependence of the peak temperature as given in the following relationship [15,24]:

$$\ln(T_p^2/\beta) = E_c/(RTp) + \text{constant} \tag{1}$$

where R is the universal gas constant. According to Eq. (1), a plot of $\ln(T_p^2/\beta)$ *versus* $1/T_p$ should be a straight line, and from its slope the value of E_c can be determined. Assuming that, usually, the change of $\ln(T_p^2)$ with β is negligibly small comparing with the change in $\ln\beta$, it is possible to write the above equation as [24]:

$$\ln\beta = -E_c/(RT_p) + \text{constant} \tag{2}$$

which should be a straight line whose slope also yields the value of E_c.

The change of $\ln(T_p^2/\beta)$ and of $\ln\beta$ *versus* $1000/T_p$ for the studied glass is shown in Fig. 5. The values of E_c, obtained according to Eq. (1), were 581 kJ/mol and 522 kJ/mol for the first and second exothermic peaks, respectively. When E_c values were determined according to Eq. (2), the values of 596 kJ/mol and 537 kJ/mol were

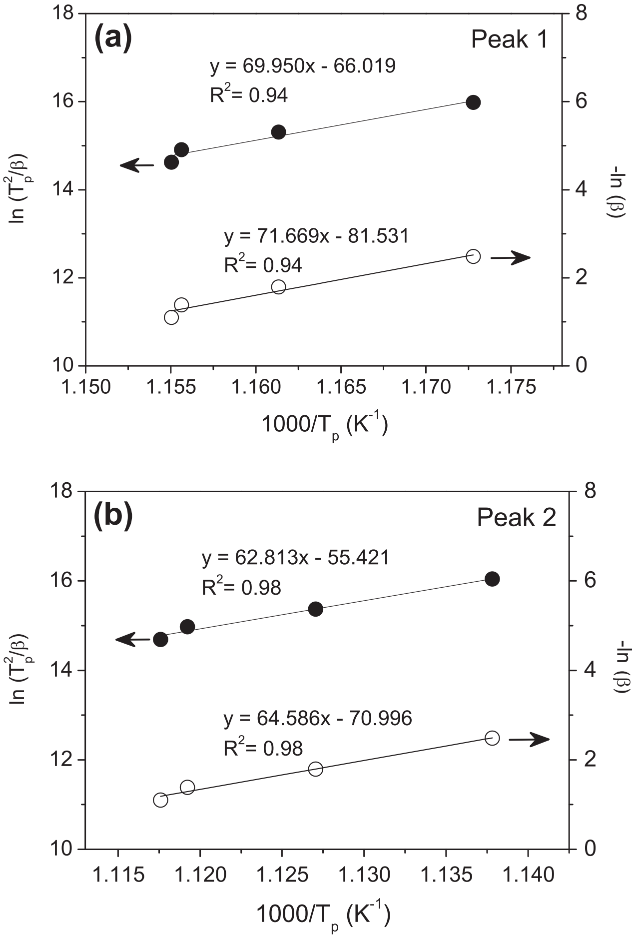

Fig. 5. Plots of $\ln(T_p^2/\beta)$ and of $\ln(\beta)$ *versus* $1000/T_p$ for the two crystallization peaks.

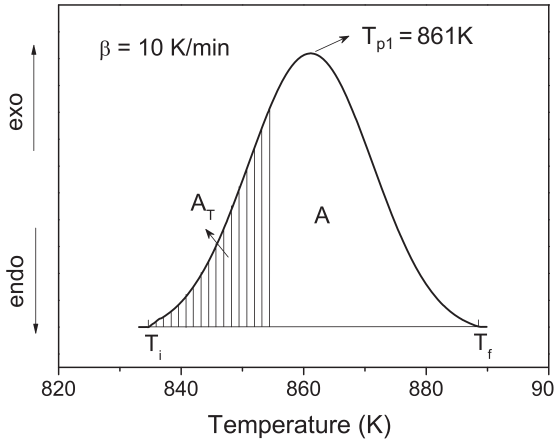

Fig. 6. Area A between T_i and T_f, and area A_T between Ti and T for the first crystallization peak ($\beta = 10$ K/min).

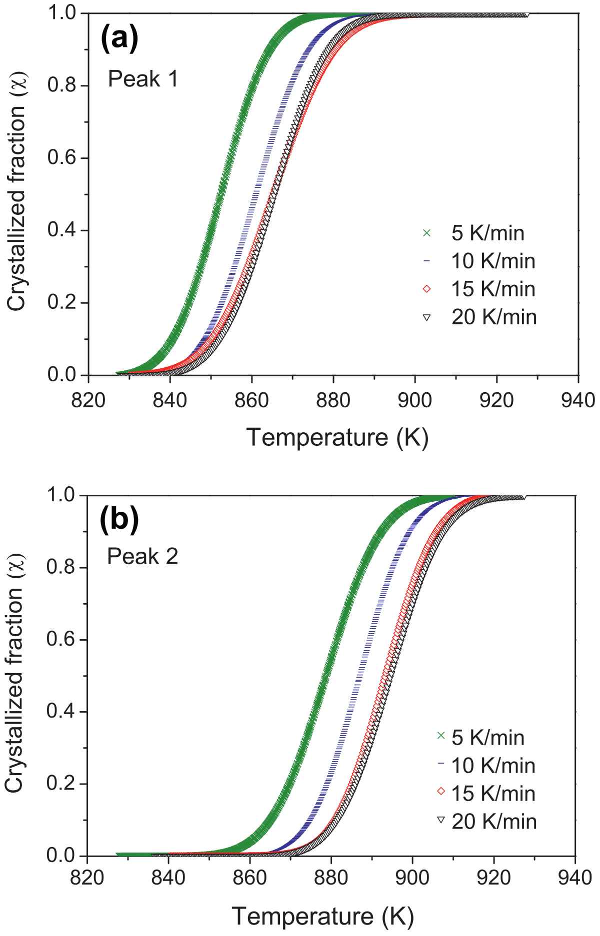

Fig. 7. Crystallized fraction as a function of temperature at different heating rates for the two overlapped crystallization peaks.

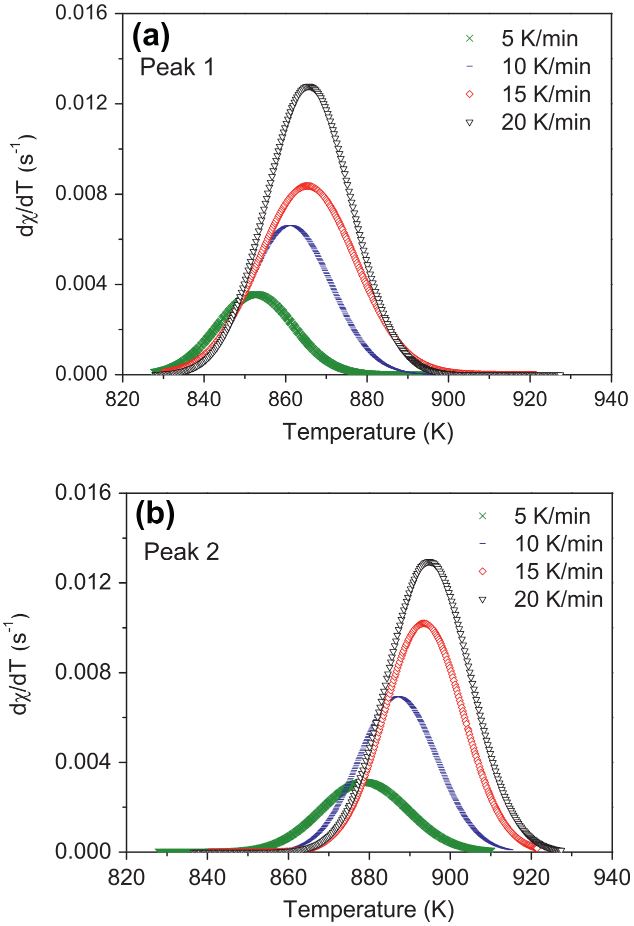

Fig. 8. Crystallization rate as a function of temperature for the first and second exothermal peaks at different heating rates.

obtained for the first and second exothermic peak, respectively. It is observed that the values of E_c calculated according Eqs. (1) and (2) are in good agreement, which indicates that it is possible to use either of the two approaches to calculate the activation energy. The activation energy of crystallization decreased for the second peak, suggesting that either the nucleation for the second crystalline phase occurred during the crystallization of the first phase, or the first phase itself provides the adequate sites for the nucleation and growth of the second phase. Thus, the value of E_c determined for the peak corresponding to barium borate (BaB_4O_7) is higher than the value of E_c determined for the peak corresponding to the crystallization of barium zinc silicate ($BaZnSiO_4$). It is considered that the composition of the residual glass after crystallization of barium borate is likely closer to that of barium zinc silicate stoichiometry because it became depleted in terms of B and Ba.

From the DTA curves the fraction of crystallization (χ) at a specific temperature can be determined [10,13,25]. The fraction crystallized at a given temperature, T, has been obtained by the ratio A_T/A, where A is the total area of the crystallization peak between the temperature T_i (where crystallization just begins) and the temperature T_f (where the crystallization is completed) and A_T is the area between T_i and T, as shown schematically in Fig. 6. The graphical representation of the volume fraction crystallized (χ) as a function of temperature (T) for both exothermic peaks shows the typical sigmoid curves for different heating rates, as presented in Fig. 7(a and b), indicating that the formation of the crystalline phase proceeds by a combination of nucleation and growth processes [26].

The ratio between the ordinates of the DTA curve and the total area of the exothermal peak gives the corresponding crystallization rates [10], which make it possible to plot the curves of the exothermal peaks presented in Fig. 8(a and b). It is observed that the maxima of ($d\chi/dt$) values, $(d\chi/dt)_{Tp}$, increase with the increase in the heating rate, as it has been reported in the literature [10,24].

From the DTA exothermic peak, the Avrami exponent (n) can be obtained by using by the following modified Ozawa equation [16,27]:

$$[d(\ln[-\ln(1-\chi)])/d(\ln\beta)]_T = -n \tag{3}$$

where χ is the volume fraction crystallized at a fixed temperature T at the heating rate β. From the value of the fraction of crystallization for each heating rate at a particular temperature, n is determined from the slopes of $\ln[-\ln(1-\chi)]$ *versus* $\ln(\beta)$, as shown in Fig. 9. As noted, the values of the Avrami exponent, n, obtained experimentally at different annealing temperatures, are 1.0 and 1.3 (mean value $\langle n \rangle = 1.2$) for the first crystallization peak, corresponding to barium borate, BaB_4O_7, and 1.5 and 2.3 (mean value $\langle n \rangle = 1.9$) for the second crystallization peak, corresponding to barium zinc silicate, $BaZnSiO_4$).

From the experimental values of $(d\chi/dt)$ at T_p, the Avrami exponent, n, can also be obtained from the following equation [10]:

$$n = ((d\chi/dt)_{T_p} \times RT_p^2)/(0.37\,\beta E_c) \tag{4}$$

The value calculated for n is very close to 1, $n \approx 1.1$, for the first peak and it is higher, $n \approx 1.4$, for the second peak. The difference between the values for n obtained from Eqs. (3) and (4) is due to the fact that n obtained from Eq. (3), modified Ozawa equation, is dependent on the temperature selected for calculation of crystallized fraction (χ) at heating rate (β), while n value obtained from Eq. (4) depends on the value of activation energy for crystallization (E_c). From the comparison of the n values determined according to Eqs. (3) and (4) with the theoretical values [12,13,18], it can be assumed that surface crystallization ($n \approx 1$) is dominant during the crystallization of barium borate and that, with further heating, during the crystallization of barium zinc silicate, the controlling mechanism evolves from surface to bulk crystallization ($n \approx 2$).

Using the experimental data presented in Fig. 7, the plots of $\ln[-\ln(1-\chi)]$ *versus* $1/T$ at the different heating rates were obtained (Fig. 10). It is noticed that in the entire range of temperatures, the plots are non-linear at all the heating rates under study. This suggests that there is a variation in E_c and n during the crystallization process of the glass [28].

The JMA model implies that the Avrami exponent n, and the activation energy E_c, should be constant during the transformation process [11]. However, some authors have shown that n and E_c values are not necessarily constant but vary during the transformation, both in isothermal [11] and in non-isothermal methods [28–30]. The activation energy for different crystallization volume fractions is not constant in the whole transformation due to the change of nucleation and growth behaviors during crystallization process [28]. The variation of the activation energy E_c and of the Avrami exponent n can be expressed by the local activation energy $E_c(\chi)$ and the local Avrami exponent $n(\chi)$ [29,30].

The local activation energy $E_c(\chi)$ can be determined from non-isothermal DTA results using the method proposed by Ozawa, according to the following relationship [28,31]:

$$[d(\ln\beta)/d(1/T)]\chi = -E_c(\chi)/R \tag{5}$$

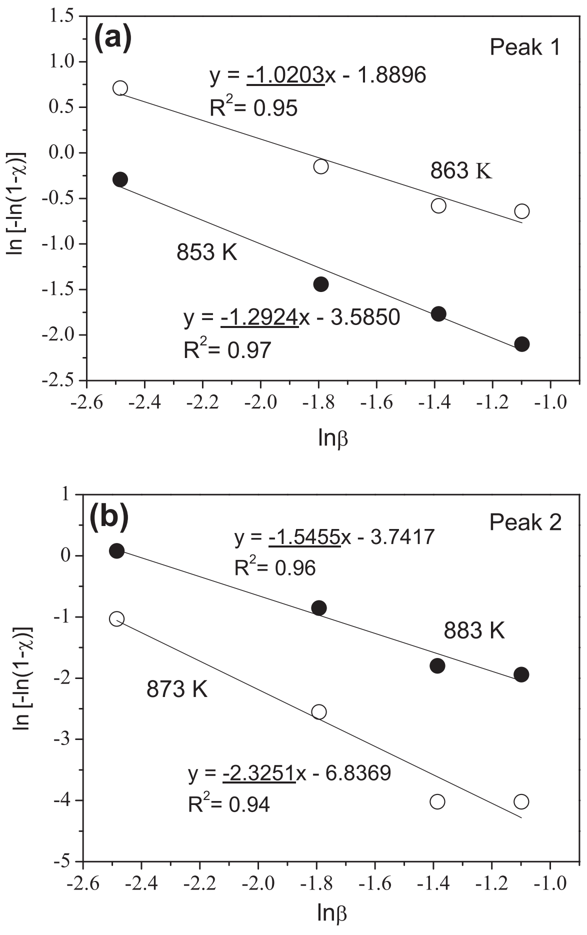

Fig. 9. Plots of $\ln[-\ln(1-\chi)]$ *versus* $\ln\beta$ for the two crystallization peaks at two different temperatures.

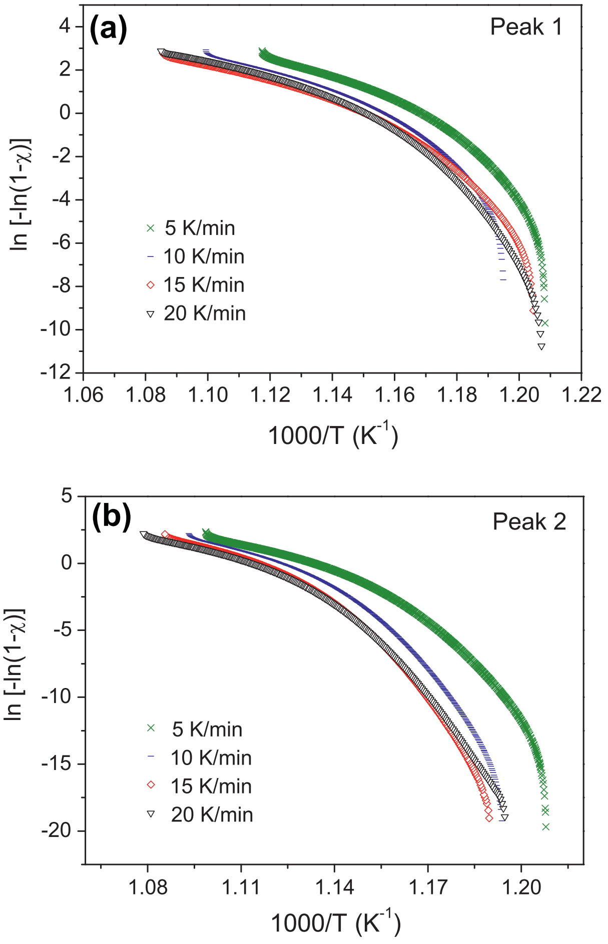

Fig. 10. Plots of $\ln(-\ln(1-\chi))$ *versus* $1000/T$ at different heating rates for the two crystallization peaks.

where R is the gas constant, T and β are the temperature and the heating rate corresponding to the value of χ. Using the experimental data presented in Fig. 7, the plot of $\ln(\beta)$ *versus* 1/T at various values of χ ($0.1 < \chi < 0.9$) was obtained (see Fig. 11), and from the slope the value of $E_c(\chi)$ was calculated.

Fig. 12 shows the variation of $E_c(\chi)$ *versus* χ for the studied glass. It is observed that for the first exothermal peak, corresponding to barium borate, $E_c(\chi)$ is higher during the initiation of the crystallization process (~700 kJ/mol), and then it decreases until ~500 kJ/mol. For the second exothermal peak, associated to the crystallization of barium zinc silicate, $E_c(\chi)$ slightly increases during the crystallization process, varying from ~490 kJ/mol up to ~570 kJ/mol. Considering the mean $E_c(\chi)$ values for the first and second exothermic peaks, (~600 kJ/mol and ~535 kJ/mol, respectively), they are very similar to E_c values (596 kJ/mol and 537 kJ/mol), calculated according to Eq. (2), where a constant activation energy *was considered* for the whole transformation process.

Considering the prior knowledge of the local activation energy for non-isothermal crystallization process, $E_c(\chi)$, it is possible to determine the local Avrami exponent, $n(\chi)$, according to the following equation [30,31]:

$$n(\chi) = (-R\partial \ln[-\ln(1-\chi)])/E_c(\chi)\partial \ln(1/T) \qquad (6)$$

Taking into account the local activation energy, $E_c(\chi)$, the local Avrami exponent, $n(\chi)$, values at a heating rate of 10 K/min were calculated using (Eq. (6)), and the change of $n(\chi)$ with χ is presented in Fig. 12. It is noticed that the local Avrami exponent increases with the crystallization fraction for BaB_4O_7 formation ($1 < n < 1.5$), and it decreases for $BaZnSiO_4$ formation ($1.7 > n > 1.4$), indicating that the primary crystallization started from the surface of the samples and with further heating evolved to the bulk.

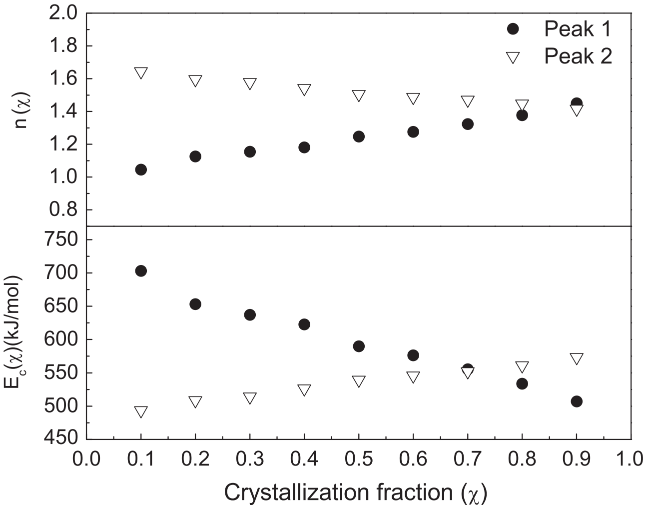

Fig. 12. Local activation energy for crystallization $E_c(\chi)$ and local Avrami exponent $n(\chi)$ as a function of crystallized fraction (χ), obtained from DTA curve at 10 K/min.

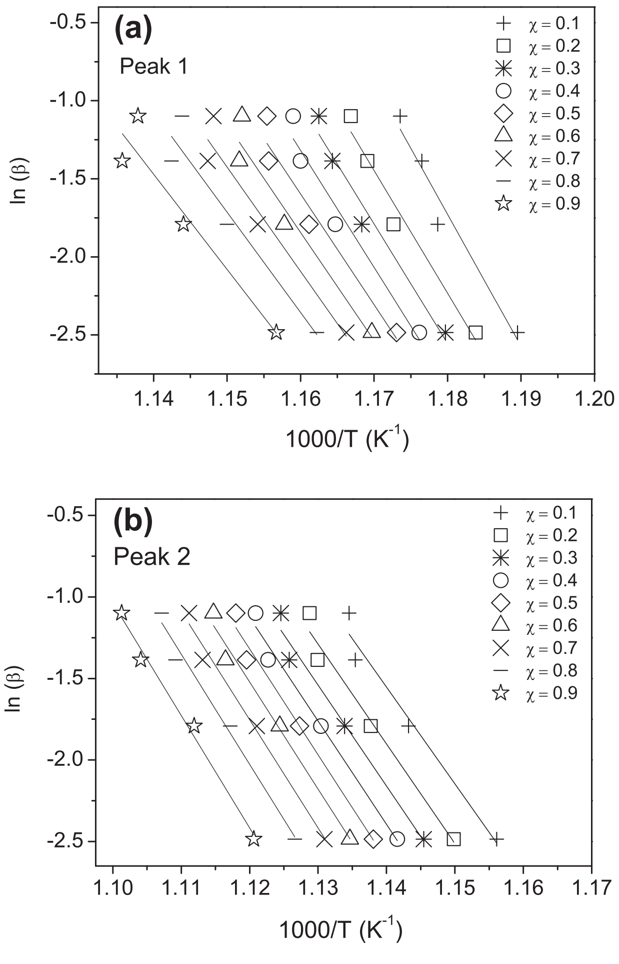

Fig. 11. Plots of $\ln(\beta)$ *versus* $1000/T$ at various values of χ ($0.1 < \chi < 0.9$) for the two crystallization peaks.

To confirm the above conclusion, the transformation from the amorphous to the crystalline state was investigated by a detailed SEM analysis of the microstructure of the sintered samples obtained after heating the compacts of glass powder with a 14.5 µm mean particle size. Fig. 13(a and b) show SEM micrographs of a glass specimen after heating at 833 K. It is observed that smooth areas, corresponding to glass, are surrounded by crystalline zones, see Fig. 13(a and b), the morphology of the crystalline phases being observed with more detail at higher magnification, Fig. 13(b). The initial glass powder particles consolidated during the heat-treatment, eliminating most of the open porosity [6], and simultaneously nucleation and crystal growth started from the surface of the glass particles, inhibiting further densification [6]. With further heating, as revealed by the SEM micrograph of a glass specimen sintered at 853 K, Fig. 13(c), crystallization proceeded towards the bulk. In fact, comparing Fig. 13(b and c), that show SEM micrographs at the same magnification, it is observed that at 833 K, Fig. 13(b), large areas of glass (corresponding to initial glass particles) are still present and that a significant amount of lamellae crystallites aligned in a particular direction covered the glass particles surface, while with further heating, at 853 K, Fig. 13(c), the formation of crystals was extended into the bulk material and much smaller residual glass areas remained in the samples when sintered at high temperature. Additionally, a small number of quasi-spherical nano-sized crystallites can be observed in sintered glass samples, as clearly shown in Fig. 13(b and c).

Chemical analysis by EDS of the crystallites with different morphological types has not been possible because their size is much smaller than the detection width (~1 µm) of the microanalysis probe [32]. However, taking into account the XRD results shown in Fig. 4, it is likely that primary crystallization started at the surface of glass particles with crystallization of lamellar barium borate crystallites that was followed by the crystallization of spherical barium zinc silicate crystallites. Moreover, the dependence of the local activation energy on the volume of the crystallized fraction suggests that a multi-step kinetic reaction took place during sintering and crystallization of the glass.

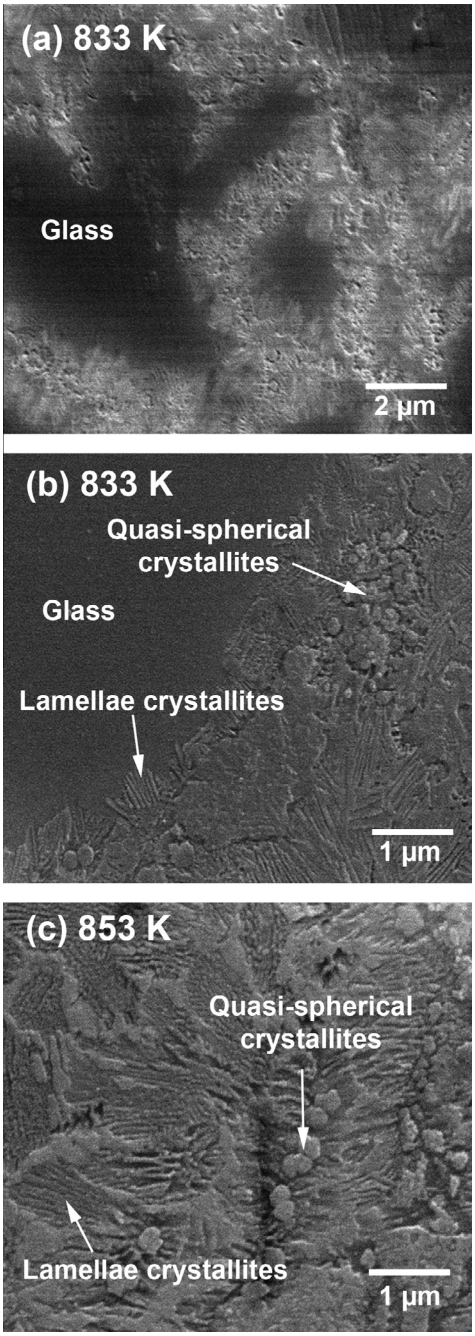

Fig. 13. SEM photographs of glass samples heated at the indicated temperature.

4. Conclusions

The crystallization kinetics of a BaO–ZnO–B_2O_3–SiO_2 glass has been studied by non-isothermal DTA, XRD, and SEM. The DTA curves exhibited a well-defined crystallization exothermal effect, which was formed by the overlapping of two exothermic crystallization peaks. The identification of the crystalline phases by XRD revealed the presence of barium borate (BaB_4O_7) together with barium zinc silicate ($BaZnSiO_4$).

The kinetic parameters have been obtained by the use of different methods. The calculated values of the local activation energy for the growth of BaB_4O_7 decreased from 700 to 500 kJ mol^{-1} and for the growth of $BaZnSiO_4$ increased from 490 to 570 kJ mol^{-1}, as the fraction of crystallization varied from 0.1 to 0.9. The calculated values for the Avrami exponent n, which were analysed together with the results from SEM observations, indicated that surface crystallization was the dominant crystallization mechanism, but while sintering temperature of the glass increased from 833 K to 853 K, crystallization progressed from the surface towards the bulk.

Acknowledgements

This work was supported by the Fundação para a Ciência e a Tecnologia (Portugal), through Project PTDC/CTM/102141/2008 and through funding to I3N/CENIMAT (Strategic Project PEst-C/CTM/LA0025/2013).

References

[1] E.-S. Lim, B.-S. Kim, J.-H. Lee, J.-J. Kim, J. Eur. Ceram. Soc. 27 (2007) 825–829.
[2] S. Chen, S. Zhang, X. Zhou, T. Zhang, M. He, J. Alloys Comp. 498 (2010) 185–190.
[3] N. Santha, S. Shamsudeen, N.T. Karunakaran, J.I. Naseemabeevi, Int. J. Appl. Ceram. Technol. 8 (2011) 1042–1049.
[4] S. Chen, D. Zhu, J. Alloys Comp. 356 (2012) 73–79.
[5] Z. Wang, Y. Hu, H. Lu, F. Yu, J. Non-Cryst. Sol. 354 (2008) 1128–1132.
[6] R.C.C. Monteiro, A.A.S. Lopes, M.M.A. Lima, J.P. Veiga, R.J.C. Silva, C. Dias, E.J.R. Davim, M.H.V. Fernandes, J. Amer. Ceram. Soc. 95 (2012) 3144–3150.
[7] G.H. Hwang, H.J. Jeon, Y.S. Kim, J. Am. Ceram. Soc. 85 (2002) 2956–2960.
[8] E.-S. Lim, B.-S. Kim, J.-H. Lee, J.-J. Kim, J. Electroceram 17 (2006) 359–364.
[9] Y. Hu, C.-L. Huang, J. Non-Cryst. Sol. 278 (2000) 170–177.
[10] A. Arora, E.R. Shaaban, K. Singh, O.P. Pandey, J. Non-Cryst. Sol. 354 (2008) 3944–3951.
[11] A.A. Abu-Sehly, S.N. Alamri, A.A. Joraid, J. Alloys Comp. 476 (2009) 348–351.
[12] M. Erol, S. Kuchukbayrak, A. Ersoy-Mericboyu, J. Non-Cryst. Sol. 355 (2009) 569–576.
[13] M. Ghasemzadeh, A. Nemati, A. Nozad Golikand, Z. Hamnabard, S. Baghshahi, Metal-Org. Nano-Metal Chem. 41 (2011) 561–570.
[14] B. Shanmugavelu, V.V.R.K. Kumar, J. Am. Ceram. Soc. 95 (2012) 2891–2898.
[15] H. Yinnon, D.R. Uhlmann, J. Non-Cryst. Sol. 54 (1983) 253–275.
[16] H.E. Kissinger, Anal. Chem. 29 (1957) 1702–1706.
[17] A. Birkan Seluk, H. Yavuz, Mater. Lett. 57 (2003) 4382–4387.
[18] D.W. Henderson, J. Therm. Anal. 15 (1979) 325–331.
[19] K. Matusita, S. Sakka, J. Non-Cryst. Sol. 38&39 (1980) 741–746.
[20] A. Arora, A. Goel, E.R. Shaaban, K. Singh, O.P. Pandey, J.M.F. Ferreira, Physica B 403 (2008) 1738–1746.
[21] A. Arora, K. Singh, O.P. Pandey, Intern. J. Hydrogen Energy 36 (2011) 14948–14955.
[22] A. Arora, V. Kumar, K. Singh, O.P. Pandey, Ceram. Int. 37 (2011) 2101–2107.
[23] C.A.C. Feitosa, V.R. Mastelaro, A.R. Zanatta, A.C. Hernandes, E.D. Zanotto, Opt. Mater. 28 (2006) 935–943.
[24] J. Vázquez, C. Wagner, P. Villares, R. Jiménez-Garay, J. Non-Cryst. Sol. 235 (1998) 548–553.
[25] C-R. Chang, J-H. Jean, J. Am. Ceram. Soc. 82 (1999) 1725–1732.
[26] J.-H. Jean, Y.-C. Fang, S.X. Dai, D.L. Wilcox, J. Am. Ceram. Soc. 84 (2001) 1354–1360.
[27] H. Chen, J. Non-Cryst. Sol. 27 (1978) 257–263.
[28] A.A. Joraid, S.N. Alamri, A.A. Abu-Sehly, J. Non-Crystal. Solids 354 (2008) 3380–3387.
[29] F. Liu, F. Sommer, C. Bos, E.J. Mittemeijer, Int. Mater. Rev. 52 (2007) 193–212.
[30] K. Majhi, K.B.R. Varma, J. Mater. Sci. 44 (2009) 385–391.
[31] T. Ozawa, J. Therm. Anal. 31 (1986) 547–551.
[32] J.I. Golstein, D.E. Newbury, P. Echlin, D.C. Joy, A.D. Romig Jr., C.E. Lyman, C. Fiori, E. Lifshin, Scanning Electron Microscopy and X-ray Microanalysis, in: A Text for Biologists, Materials Scientists, and Geologists, Plenum Press, New York, 1992, pp. 417–522.